VOL. 9, NO. 1, JANUARY 2014 ISSN 1819-6608
ARPN Journal of Engineering and Applied Sciences


www.arpnjournals.com

NUMERICAL ASSESSMENT OF MATERIAL MISMATCH EFFECT OVER MODE I CRACK TIP ZONES IN GLARE

Sunil Bhat and S. Narayanan
School of Mechanical and Building Sciences, VIT University, Vellore, Tamil Nadu, India
E-Mail: kbbrp@rediffmail.com

ABSTRACT

The nature and the size of Mode I crack tip zones developing in cracked fibre metal laminate, Glare, (Aerospace aluminum alloy layers + fibre and resin based prepregs) when subjected to far field load differ from those in similarly loaded cracked plain aerospace aluminum alloy specimen due to amplification or reduction in crack tip stress field of the laminate that is caused by load transfer effect because of property mismatch between un-identical materials in the laminate. This difference is assessed by finite element method in the paper. Glare laminates with two types of Mode I crack orientations are investigated – Type I in which the Mode I crack in outer aluminum layer is normal and near to the prepregs and Type II in which the Mode I cracks run across the aluminum layers in presence of delaminations at aluminum-fibre interfaces. Two different laminate curing temperatures of 90 deg. C and 120 deg. C are separately considered in the analysis to estimate the influence of residual stress over crack tip characteristics. Monotonic tensile stress of 150 MPa is applied over the laminates. Identically, cracked and stressed, plain aerospace aluminum alloy specimens are also modeled for the purpose of comparison of their results with those of the laminates. The intensity of stress fields near Mode I crack tips in the laminates is observed to be different than that near crack tips in plain aluminum specimens - amplified in Type I and diminished in Type II laminates. Consequently, the size and the shape of crack tip zones in laminates vary from those in plain aluminum specimens. Values of J integrals near crack tips are also found to be more and less than the induced J values in Type I and Type II laminates respectively that support the amplification and shielding effects at the crack tips in the laminates.

Keywords: glare, 2024-T3 aerospace aluminum alloy, crack tip zones, elasticity, fibre metal laminate, J integral, load transfer, material mismatch, mode I crack, plasticity.

1. INTRODUCTION

Fibre metal laminate (FML) is an advanced hybrid material system that consists of layers of thin and light metallic sheets alternately bonded with composite prepregs by heat and pressure, each prepreg built up of several, resin impregnated, uni-directional fibres laid in similar or different orientations. Besides offering gain in specific strength, FML's exhibit excellent fatigue and fracture resistance that is useful in aerospace applications. Glare, one such FML comprising aerospace aluminum alloy and glass fibre based prepregs, is taken up for investigation in the present work.

Multiple property mismatched interfaces exist in Glare due to the presence of different material layers with constituents on either side of each interface having un-identical elasticity and plasticity properties. Also, the magnitude of residual stress, that develops in material layers during laminate curing, vary due to different stiffness and coefficients of thermal expansion of the materials. Consequently from mechanics point of view, the induced stress state that develops in material layers of un-cracked Glare when subjected to uniformly applied or far field stress differs from the applied stress due to inherent residual stresses existing in the laminate and redistribution of applied stress for fulfillment of the continuity of displacement across the elasticity mismatched interfaces in order to maintain same strain in all the material layers of the laminate. Stress state in the laminate further changes in presence of cracks that nucleate and grow in weak aluminum layers while ultra strong fibres don't fracture and remain intact. Refer Figure-1. Two types of cracked Glare are examined *viz*. Type I in which a small size, through, Mode I edge crack in outer aluminum layer is normal to the interface of prepregs and Type II in which, through, Mode I edge cracks in aluminum layers are oriented normally across the interfaces of prepregs, the latter type being more common. As the Mode I crack advances towards the interface of first prepreg in Type I laminate, the mismatch in shear/elastic modulus between parent aluminum and affected material layers on other side of the interface begins to influence the crack tip characteristics. Load is transferred towards the crack tip due to higher shear modulus of parent aluminum than that of influencing layers on other side of the interface that changes the stress values from the induced state which manifests in the form of amplified stress field at the crack tip. The crack on nearing the interface begins to experience the effect of plasticity mismatch between the materials as well as soon as the small plastic zone ahead of the crack tip touches the interface. Sudden reduction in stress field, leading to crack tip shielding, follows when the tip touches the soft thin resin layer of the prepreg. The crack after propagating through resin is finally deflected as the, Mode II, interfacial crack along the interface of non-penetrative fibre wall. On the other hand, the normal, Mode I, edge cracks in Type II laminate are continuously shielded during their growth due to load transfer away from them towards stronger fibres that diminishes the stress states at crack tips, the phenomenon commonly known as fibre bridging. The cracks in such laminates can

either propagate as tunnels without the formation of transverse, Mode II, interfacial cracks at aluminum-fibre interfaces or can grow along with the interfacial cracks in the form of a balanced and coupled process resulting in the formation of delaminations, the latter case being considered in the present work. Interfacial cracks nucleate when shear stresses at aluminum-fibre interfaces exceed the strength of bonding resin. Delaminations of different shapes can develop, the contour of the delamination edge or debonding curve joining the tips of normal and interfacial cracks being decided by the difference in growth rates of the cracks that in turn depends upon the material properties and the applied load parameters.

Stress amplification or reduction at Mode I crack tip in Glare, caused by load transfer due to material mismatch, affect the characteristics of crack tip zones as well. The aim of the paper is to numerically verify the material mismatch effect by assessing the nature and the size of Mode I crack tip zones in the laminate. Both the stated types of cracked Glare are modeled by finite element method under far field stress of 150 MPa. Two different laminate curing temperatures of 90 deg. C and 120 deg. C are assumed in the analysis to estimate the influence of residual stress over crack tip zones. Identically stressed, plain aerospace aluminum alloy specimens, with dimensions and crack configurations similar as that of the laminates, are also modeled to compare the crack tip zones in them with those in the corresponding laminates. The size and the nature of crack tip zones in the laminates are clearly found to be different than those in plain aluminum specimens due to load transfer effects existing in the former that are missing in the latter. Values of energy release rates are also obtained in the form of J integrals over various paths near crack tips in the laminates. They too are found to deviate from the induced values, higher in Type I laminate due to crack tip stress amplification and lower in Type II laminate due to crack tip stress reduction.

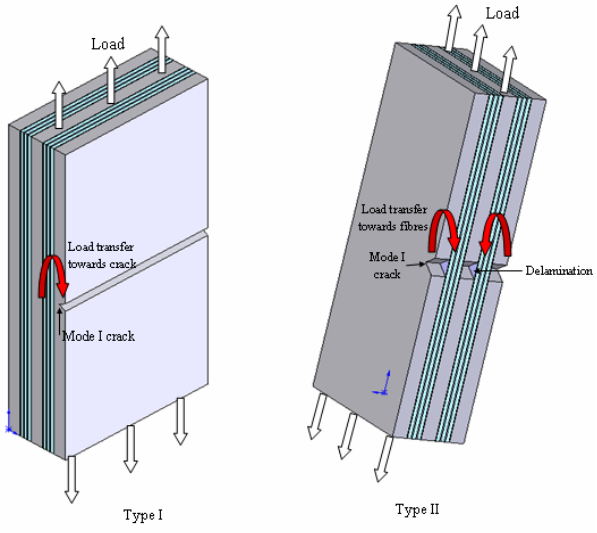

Figure-1. Investigated laminates.

2. LITERATURE REVIEW

Numerical treatment of normal, Mode I, cracks in layered, multi-material, composites as Type I laminates has been successfully carried out previously by Kim *et al*. [1] who modeled a normal crack approaching multiple, compositionally graded, inter-layers by finite element method to estimate the effect of interfaces over the crack tip. They also assessed the global and local fracture aspects numerically [2]. But the material layers in the examinations were mostly elastically identical with only strength mismatch existing between them. Work is also reported, albeit limited in nature, over Mode I cracks in multi-layered composites containing materials that have both elasticity and plasticity mismatches. For instance, experimental work by Milan and Bowen [3] on fatigue crack growth towards the interface between stronger composite of aluminum 2124 alloy + 35% SiC and weak plain aluminum 2124 alloy indicated that the elasticity and plasticity mismatch between the materials caused stress amplification or shielding effects at the crack tip leading to increased or reduced fatigue crack growth rates respectively. Crack tip stress field intensified when the crack in stronger composite grew towards the interface of weak plain aluminum whereas the crack tip stress field diminished when the crack approached the interface of stronger composite from weak plain aluminum side. Numerically, the normal crack near the interface between overmatched and undermatched welds, possessing both the types of mismatches, was modeled by Predan *et al*. [4] to obtain the difference between the applied and crack tip J integral values. Off late, Bhat and Patibandla [5] have reported theoretical and numerical analysis of Mode I crack in aluminum layer growing normally towards elasticity and plasticity mismatched interfaces of composite prepregs to assess the effect of interfaces on crack tip parameter. Unlike Type I laminates, several fatigue and fracture studies have been reported on, Mode I, cracked Type II laminates under various types of load spectrum and operational conditions, notably by Guo *et al*. [6, 7, 8], Alderliesten *et al*. [9, 10, 11, 12] etc., that have confirmed crack tip shielding due to fibre bridging and therefore enhanced fatigue life of such laminates. It is confirmed from the literature survey that although the models for obtaining crack tip parameter in multi-material laminates are available, there exists the need for in-depth examination of the behavior of crack tip zones in them under the influence of property mismatch effects. The results are best visualized by comparing the crack tip zones in the laminates with those in plain homogenous specimens that are made of metal used in the laminate and in which the mismatch effects don't exist. The present paper is an attempt in that direction.

3. GLARE FEATURES

Refer Figure-2. Glare laminate is assumed to made of three, 0.4 mm thick, 2024-T3 aerospace aluminum alloy sheets bonded alternatively with two prepregs, each prepreg built up of three composite layers in the sequence, c0-c90-c0. A composite layer consists of

4 mil or 0.1mm thick unidirectional E-glass fibre cloth that is coated on both the sides with a thin layer of epoxy resin. Volume fractions of fibre and resin in the composite layer are 0.751 and 0.249, respectively. Composite c0 has fibres laid in *y* direction i.e., along the direction of the load whereas composite c90 has fibres laid in *x* direction i.e. perpendicular to the direction of the load. The laminate is 200 mm long, 50 mm wide (*w*) and 2 mm thick (*d*). Standard material properties are displayed in Table-1. The coefficients of thermal expansion of the laminate in longitudinal (*y*) direction, α_{ll}, and in transverse (*x*) direction, α_{tl}, are found to be of the order of $18.62\times10^{-6}\,C^{-1}$ and $18\times10^{-6}\,C^{-1}$ respectively from conventional formulations related to composites and laminates. These coefficients are required to estimate the curing or residual strain in each material layer. Residual stress values in material layers are then obtained from the product of residual strain and stiffness matrix of respective materials under plane strain and plane stress conditions in Type I and Type II laminates respectively.

Two laminate curing temperatures of 90 deg. C and 120 deg. C are considered separately in the analysis to estimate the influence of residual stress over crack tip characteristics. Far field, monotonic, tensile stress, $\sigma_{y,applied}$, of 150 MPa is applied over the laminates in *y* direction. Classical theory of laminates is employed to obtain the strain, under applied stress, in the laminate that is same in all the material layers. Product of laminate strain and respective material stiffness matrix provides the redistributed applied stress in each material layer. Induced stress state, $\sigma_{induced}$, in the material layers is obtained by superimposing residual stress and redistributed stress in the layers. Values of $\sigma_{induced}$, with and without the presence of residual stress, are available at Appendix A. Since the coefficient of thermal expansion of aluminum, α_{al}, is greater than that of fibre, α_f, residual stress in *y* direction is tensile in aluminum layers and compressive in fibre layers. $\sigma_{induced}$ further deviates in cracked laminates, especially near crack tips, due to load transfer effects stated in Section 1. The final stress state, σ_{total}, in cracked laminates is obtained from the finite element analysis.

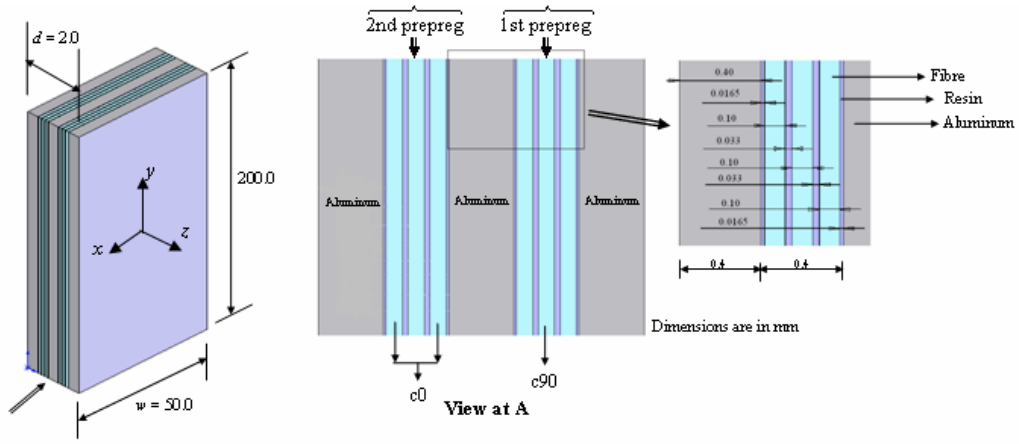

Figure-2. Construction of glare.

Table-1. Material properties.

Property	**Aluminum 2024-T3 alloy, *al*** (Isotropic)	**E-Glass, *f*** (Isotropic)	**Epoxy resin, *r*** (Isotropic)
Modulus of elasticity, MPa	72000.0	71000.0	3500.0
Shear modulus, MPa	27060.0	29710.0	1250.0
Poisson's ratio, υ	0.33	0.22 (Major)	0.33
Yield strength (Y), MPa	345.0	---	---
Ultimate tensile strength (*UTS*), MPa	485.0	3450.0	60
Percent elongation	18.0	4.8	4.0
Coeff. of thermal expansion (α), C^{-1}	23×10^{-6}	5.0×10^{-6}	57.5×10^{-6}
Plane strain fracture toughness, $MPa\sqrt{m}$	40.0-50.0	4.0-5.0	0.5-0.7

4. THEORETICAL REVIEW

Like in any homogeneous body, various stress zones develop near Mode I crack tip in loaded Glare laminate. The size of these zones is the measure of the intensity of stress field near the crack tip. The highly stressed region immediately ahead of the crack tip, where material degradation or damage occurs, is known as the process or fracture zone. Micro-mechanical processes create new traction free surfaces in the form of mini voids/cracks in this zone that coalesce with the parent crack. Material yielding outside the process zone, where the stress level exceeds the material elastic limit, is referred as the plastic or yield zone. The plastic zone in turn is surrounded by an elastic zone where the stress level is within the material elastic limit. Identification of location and size of process, plastic and elastic zones in each material layer is carried out by employing the conditions, $\sigma_{y,total} > UTS$, $UTS > \sigma_{y,total} > Y$ and $Y > \sigma_{y,total} > \sigma_{y,induced}$, respectively where $\sigma_{y,total}$ is the final stress state in load line (*y*) direction in selected material layer around crack tip that, as stated earlier, differs from stress field away from the crack tip, $\sigma_{y,induced}$. Energy release rate parameter, *J* integral, is valid in both small scale yielding (SSY) and higher yielding conditions (Elastic-plastic fracture) at the crack tip. Use of stress intensity parameter, *K*, is justified in the case of SSY condition. Since the fracture characteristics of the laminates are compared with those of identically stressed and cracked plain aluminum specimens in SSY condition in the present work, the well known theoretical formulations governing plain or homogenous aluminum specimens in SSY condition are briefly reviewed as follows keeping in view the fact that the far field stress applied over the plain aluminum specimens in *y* direction is equal to the induced stress in aluminum layer of the laminate, $\sigma_{y,induced,al}$, to simulate identical load conditions over cracks in plain aluminum specimens and in the laminates. The formulations are subsequently checked for applicability to laminates.

i) Plain aluminum specimen with similar crack configuration and load as in Type I laminate

(Plain strain condition)

For Mode I crack of length, *c*, with plastic zone of size, *r*, at its tip, the effective crack length, c_{eff}, to account for crack tip plasticity is given by $c+\frac{r}{2}$. If $r << c$ in SSY, $c_{eff} \approx c$ and induced stress intensity parameter, $K_{induced}$, assumes the conventional form $K_{induced} = \sigma_{y,induced,al} \times \sqrt{\pi c} \times CF$ where configuration factor, *CF*, of an edge crack is empirically approximated by $CF = \left[1.12 - 0.23\frac{c}{d} + 10.55\left(\frac{c}{d}\right)^2 - 21.72\left(\frac{c}{d}\right)^3 + 30.39\left(\frac{c}{d}\right)^4\right]$. The size of Dugdale's crack tip plastic zone, $\bar{r}$, is determined from $\bar{r} = \frac{\pi}{8}\left(\frac{K_{induced}}{\sqrt{3}Y_{al}}\right)^2$. Elastic zone size along crack axis, $\bar{x}$, is estimated from $\bar{x} = \frac{1}{2\pi}\left(\frac{K_{induced}}{\sigma_{y,induced,al}}\right)^2$. Induced value of *J* integral is given by $J_{induced} = \frac{(K_{induced})^2(1-\upsilon_{al}{}^2)}{E_{al}}$. *J* integral at the crack tip, J_{tip}, over cyclic path *P* [13] near crack tip is obtained from, $J_{tip} = \int_P (W_e dy - T_z \frac{\partial w_n}{\partial z} ds - T_y \frac{\partial v_n}{dz} ds)$, where W_e represents strain energy density, w_n and v_n as the nodal displacements in *z* and *y* directions and traction terms $T_z = \sigma_z n_z + \tau_{zy} n_y$, $T_y = \sigma_y n_y + \tau_{zy} n_z$ with *n*'s in traction terms denoting unit vectors in the directions indicated at corresponding subscripts. Crack tip stress intensity parameter, K_{tip}, and J_{tip} are related by $K_{tip} = \sqrt{J_{tip} \times \frac{E_{al}}{(1-\upsilon_{al}{}^2)}}$.

ii) Plain aluminum specimen with similar crack configuration and load as in Type II laminate

(Plain stress condition)

For Mode I crack of length, *c*, $K_{induced} = \sigma_{y,induced,al} \times \sqrt{\pi c} \times CF$ where $CF = \left[1.12 - 0.23\frac{c}{w} + 10.55\left(\frac{c}{w}\right)^2 - 21.72\left(\frac{c}{w}\right)^3 + 30.39\left(\frac{c}{w}\right)^4\right]$. The size of Dugdale's plastic zone is given by $\bar{r} = \frac{\pi}{8}\left(\frac{K_{induced}}{Y_{al}}\right)^2$ whereas the elastic zone size at the crack tip is again written as $\bar{x} = \frac{1}{2\pi}\left(\frac{K_{induced}}{\sigma_{y,induced,al}}\right)^2$. $J_{induced} = \frac{(K_{induced})^2}{E_{al}}$ and $J_{tip} = \int_P (W_e dy - T_x \frac{\partial u_n}{\partial x} ds - T_y \frac{\partial v_n}{\partial x} ds)$ where u_n and v_n are the nodal displacements in *x* and *y* directions, $T_x = \sigma_x n_x + \tau_{xy} n_y$ and $T_y = \sigma_y n_y + \tau_{xy} n_x$. Finally, $K_{tip} = \sqrt{J_{tip} \times E_{al}}$.

iii) Laminates

The equations for $K_{induced}$ stated above remain same in the laminates containing cracks in parent aluminum layers under SSY condition. Unlike plain

aluminum specimens where $K_{tip} = K_{induced}$, $K_{tip} \neq K_{induced}$ in the laminates due to load transfer effect over the crack tips. Load or energy transfer, quantified by $J_{interface}$, changes K_{tip} in compliance with the conservation of energy release rate criterion, $J_{induced} = J_{tip} \pm J_{interface}$ where +ve sign holds good when the crack in soft and weaker material faces the interface of stiff and stronger material and vice versa in the case of -ve sign. Consequently, the expressions for sizes of crack tip zones in the laminates differ from those in plain aluminum specimens. Since in Type I laminate, the crack tip zones, besides in parent material, develop in different interface materials as well e.g. the spread of elastic zone across the interface in the present case, their sizes are difficult to be obtained theoretically with precision and are obtained numerically. On the other hand, as crack tip zones in Type II laminate are confined to aluminum layer alone, their sizes can be theoretically determined upon replacing $K_{induced}$ with K_{tip} in the equations stated for plain aluminum specimen. Expressions for J_{tip} remain the same in both the types of laminates as in the plain aluminum specimens.

5. FINITE ELEMENT MODELING

2D, finite element model of Type I laminate is created with 8 noded, solid 183 elements in aluminum layers and 8 noded solid shell 281 elements in resin and fibre layers under plane strain condition. Number of elements and nodes in the model are 40912 and 123727 respectively. Mode I cracks of 0.17 mm, 0.24 mm, 0.305 mm, 0.365 mm and 0.4 mm size (*c*) are modeled by node release method. Likewise, 3D model of Type II laminate is created with 8 noded, solid 185 elements in aluminum and 8 noded, layered solid shell 190 elements in fibre and resin layers. 3D modeling is adopted in this laminate in order to model the delaminations. Number of elements and nodes in the model are 55827 and 53066, respectively. Delaminations comprising normal (Mode I) and interfacial (Mode II) cracks of 25 mm (*c*) and 9.4 mm (*b*) sizes, respectively [10] are modeled by 8 noded, inter 205 cohesive elements. Laminates of double delamination type (Mode I cracks in two aluminum layers with two interfacial cracks) and multiple delamination type (Mode I cracks in all three aluminum layers with four interfacial cracks) are investigated. Different debonding curves, leading to dissimilar delamination shapes, are assumed to be of linear, cosine, parabolic and elliptical types that are considered separately in both double and multiple delamination type laminates. Values of maximum normal traction, σ_z, width and maximum equivalent shear traction of τ_{zy} and τ_{zx} in the delamination zone are input as C1, C2 and C3 respectively in, traction and separation distance type, cohesive element code. Since the type of de-bonding curve influences the cohesive element data, albeit marginally, the data are found for each of them by modeling cracked laminates without delaminations but with the use of a chosen debonding curve to record the maximum values that develop just ahead of the curve. Sample values of C1, C2 and C3 in the laminate cured at 120 deg. C, with double delamination of triangular shape (linear debonding curve) are of the order of 19.5 MPa, 0.001 mm and 15.03 MPa, respectively.

Half of the laminates are only modeled due to the symmetry of applied load and laminate geometry. Stress-strain data of materials, provided at Figure-3, are used in the material models. Non-linear data is used in aluminum and resin layers. Monotonic tensile stress, $\sigma_{y,applied}$, of 150 MPa is applied at the top edge of the laminate in *y* direction while the residual stress, whose values in individual layers are taken from Appendix A, are introduced over respective nodes in *x* and *y* directions of the models. In Type I laminate, the bottom nodes on cracked aluminum layer are unconstrained while all other nodes ahead of the crack tip along the laminate thickness are constrained in *y* direction ($v = 0$). In Type II laminate, the bottom nodes on all cracked aluminum and resin layers are unconstrained while the nodes, along the width, on un-cracked fibre throughout and on un-cracked aluminum and resin layers ahead of crack tip are constrained in *y* direction. The nodes are thoroughly checked for connectivity before executing the models for solution. Use of higher order elements ensures quick convergence. Mesh models of the laminates are displayed at Figure-4. Equivalent plain 2024-T3 aerospace aluminum alloy specimens with similar dimensions and Mode I crack configurations as of Type I and Type II laminates, under applied stress equal to induced stress in aluminum layers of the laminates, $\sigma_{y,induced,al}$, in 90 deg. C and 120 deg. C cured cases are also modeled in plane strain and plane stress conditions. Since *J* integral method, that does not critically depend upon the type of mesh, is used to obtain the crack tip energy release rate, a simpler rectangular mesh is employed instead of singular element mesh at the crack tips.

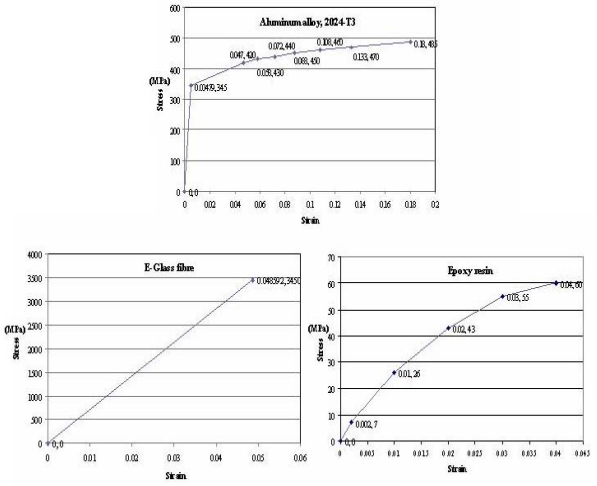

Figure-3. Stress-strain plots of material.

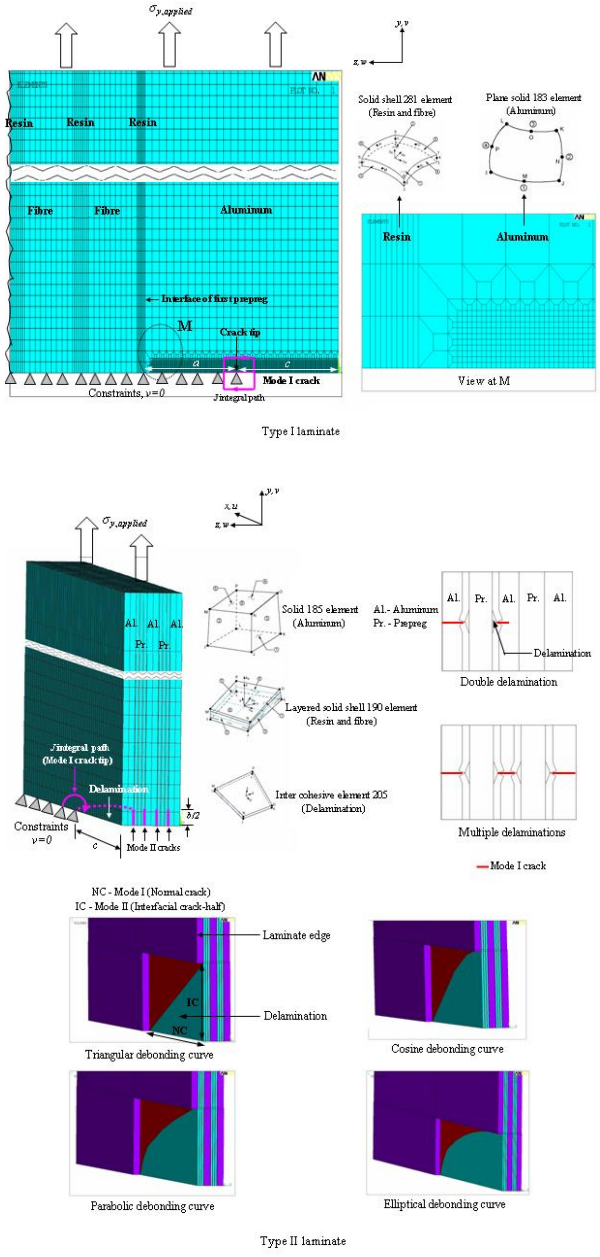

Figure-4. Mesh models of laminates.

6. RESULTS AND DISCUSSIONS

Values of $\sigma_{y,induced}$ far away from the Mode I crack tip in all the material layers, provided at Appendix A, are found to be close to the finite element results of both 90 deg. and 120 deg. cured Type I and Type II laminates. This confirms the correctness of finite element models and theoretically estimated stress values. Salient results upon comparing the Mode I fracture characteristics of laminates with those of corresponding plain aluminum specimens are discussed in the following sections.

i) Type I laminate vis-à-vis plain aluminum alloy specimen

Finite element stress plots of the laminate in load line direction, $\sigma_{y,total}$, at few selected crack lengths are sequentially presented in Figure-5 for both 120 deg. C and 90 deg. C cured cases. Stress plots of corresponding plain aluminum specimen are also displayed. The elastic zone in the laminates is found to reach up to second layer of aluminum at lower crack lengths with all resin and fibre layers of the first prepreg elastically affected. At higher crack lengths, the elastic zone spreads laterally, in load line direction, in second aluminum layer with its effect reaching to second prepreg as well. The plastic zone that remains confined to first, cracked, aluminum layer at lower crack lengths develops in second aluminum layer as well at higher crack lengths. The process zones are observed in cracked aluminum and neighboring resin layers at all the crack lengths. Numerical elastic and plastic zones, whose sizes along the crack axis, are denoted by x and r in the laminate and x' and r' in plain aluminum specimen, are highlighted in Figure-5 (r represents the size of plastic zone in cracked aluminum layer only). Refer Figure-6(a). Fulfillment of the condition, $r < c$, supports small scale yielding (SSY) condition at the crack tips in the laminates, albeit marginally, since r is not very less than c. However, the values of $\frac{\sigma_{y,induced,al}}{Y_{al}}$ in 120 deg. and 90 deg. cured laminates are equal to 0.69 and 0.63 that are reported to cause a deviation of only around 5% from the results of LEFM for a small crack [14]. So use of K appears feasible. In addition, J integral that considers the effects of higher crack tip plasticity is also employed at crack tips in the laminates. The term $2.5\left[\frac{K_{tip}}{Y_{al}}\right]^2$ is found to be less than, w, at all crack lengths that validates plane strain condition. In plain aluminum specimens, numerical value of plastic zone size, r', is slightly more than theoretical value, $\bar{r}$, although the difference increases at higher crack lengths particularly in specimens equivalent to 120 deg. cured laminate. Numerical value of elastic zone size, x', Figure-6(b), is also found to be consistently higher than the theoretical value, $\bar{x}$. These deviations are attributed to small thickness, d, and associated constraint effects of the specimen that are included in the numerical model but are not accounted for in the theoretical formulations. Overall, the order of magnitude of the values is along the expected lines. Such comparisons in plain aluminum specimens are undertaken to ascertain the results from finite element model.

Crack tip elastic zone shapes at each crack length in the laminate at each curing temperature (Figure-5) differ from those in plain aluminum specimen. Difference in shapes is due to changed stress states near crack tips in the laminates that are caused by material mismatch effects over the crack tips. Values of x are nearly similar to x' at

all the crack lengths (Figure-6(b)). Values of *r* are also nearly same as r' at initial crack lengths before *r* at higher crack lengths equals *a* i.e. the distance of crack tip from the interface due to the presence of non-penetrative fibre wall of the first prepreg that causes lateral or upward flare of the plastic zone in the first aluminum layer coupled with development of a new small plastic zone in second aluminum layer of the laminate (Figure-6a). Fulfillment of the conditions, $x \approx x'$ and $r \approx r'$, irrespective of small, load line, induced stress values in fibres due to large compressive residual stress in them, that is evident by $\sigma_{y,induced,f} < \sigma_{applied}$ at Appendix A, hint at load transfer towards the cracks in laminates at both curing temperatures. Importantly, the process zone is found to develop at crack tips in the laminates at all the crack length that does not happen in plain aluminum specimens. This convincingly confirms the role of compliant interface materials in load transfer towards crack tips in the laminates resulting in stress amplification at the tips. Refer Figure-7. J_{tip} is also found to be higher than $J_{induced}$ at all the crack lengths in both 90 deg. C and 120 deg. C cured laminates, which further supports the phenomenon of load transfer resulting in increase in energy release rate at the crack tip. The crack tip is however shielded when it touches the interface of soft resin of the pre-preg that is evident by J_{tip} being less than $J_{induced}$ at that position.

ii) Type II laminate vis-à-vis plain aluminum alloy specimen

Finite element plots of stress state in load line direction of a cracked aluminum layer, $\sigma_{y,total,al}$, in, 120 deg. and 90 deg. cured, double and multiple delamination type laminates with different delamination shapes are presented in Figure-8. Plot of plain aluminum specimen, equivalent to 90 deg. C laminate, is also provided. Convergence of solution could not be achieved in plain aluminum specimen equivalent to 120 deg. C laminate (subjected to larger applied stress of 212.6 MPa) because of the realization of limit load conditions caused by plastic collapse or excessive yielding in un-cracked ligament of length, *w*-*c*, in the specimen. Refer Figure- 9(a). The condition, $r << c$, is adequately satisfied in such laminates that confirms SSY condition and *K* dominance in them. The term, $2.5\left[\frac{K_{tip}}{Y_{al}}\right]^2$, is more than the thickness of aluminum layer in all the cases that validates plane stress condition. Since the values of *r*, in each delamination shape, are found to be much less in laminates with multiple delaminations than in those with double delamination, fibre bridging is more in the former than in the latter. The values of *r* are higher in 120 deg. C cured than in 90 deg. C cured laminates. Likewise, in each delamination type, triangular delamination results in maximum bridging and elliptical delamination the least as the values of *r* are found to be minimum in the former and maximum in the latter in both double and multiple delamination type laminates. Similar trends are observed with elastic zone, *x*, in the laminates (Figure-9(b)). It is well known that delaminations diminish fibre bridging and divert load back towards Mode I cracks which implies that the extent of Mode I crack tip zones should have been higher in multiple delaminations than in double delamination type laminates. But reverse is observed from the results. This is attributed to damage symmetry in the laminate with multiple delaminations that transfers more energy towards interfacial, Mode II, crack tips than towards Mode I crack tips. In comparison with plain aluminum specimens, *r* is much less than r' in all the cases of the laminates. This indicates load transfer away from the crack towards the fibres in the laminates resulting in reduced values of *r* and onset of crack tip shielding. Similar trends are observed by comparing elastic zone sizes (Figure-9(b)). Value of *x*, with each delamination shape, is of almost similar magnitude as x' in double delamination but much lesser than x' in multiple delaminations. Contrary to Type I laminate, the process zone is observed to develop in plain aluminum specimen but not in the laminates that confirm crack tip shielding in the latter. Refer Figure-10. J_{tip} values in general, for each delamination shape, are more in laminate with double delamination than in multiple delamination type and higher in 120 deg. C cured than in 90 deg. C cured cases. The values, for each curing temperature and delamination type, are minimum in the case of triangular delamination and maximum in the case of elliptical delamination. Finally, J_{tip} is much less than $J_{induced}$ in all the cases which once again corroborates crack tip shielding in the laminates resulting in their improved fatigue and fracture properties. Interestingly, the value of $J_{induced}$ in the laminate is much higher than critical value, J_c, of plain aluminum. But the cracks in aluminum layers of the laminate do not become critical because of load transfer towards fibres leading to much reduced and nearly safe values of J_{tip}.

Type I laminate
c - 0.17 mm

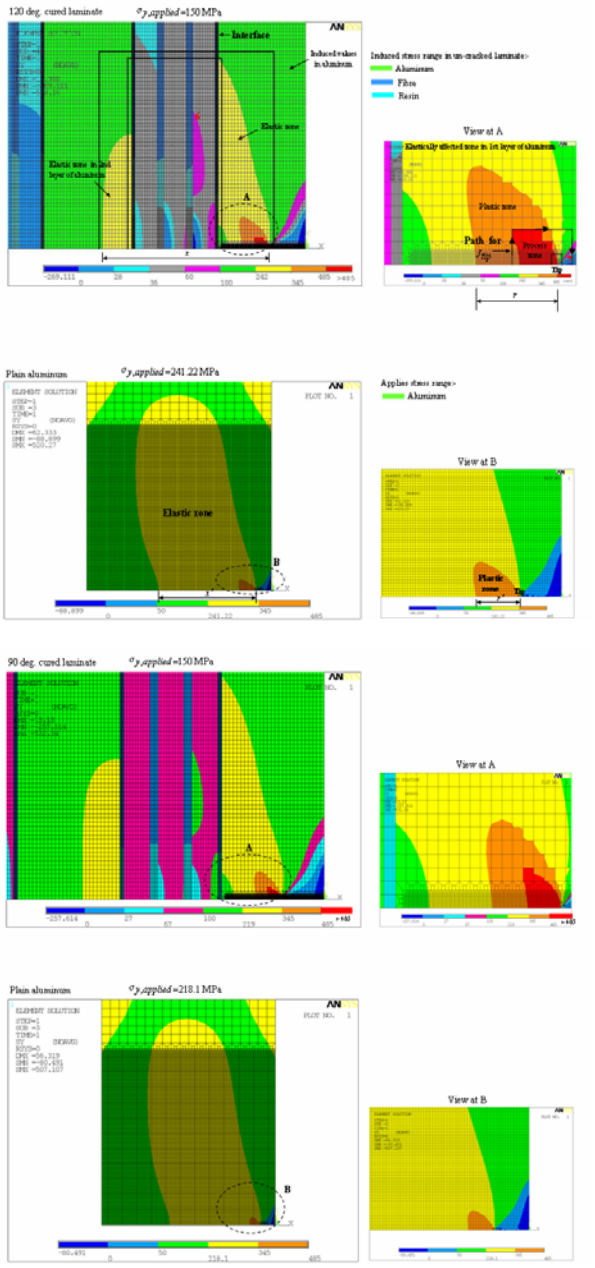

c - 0.365 mm

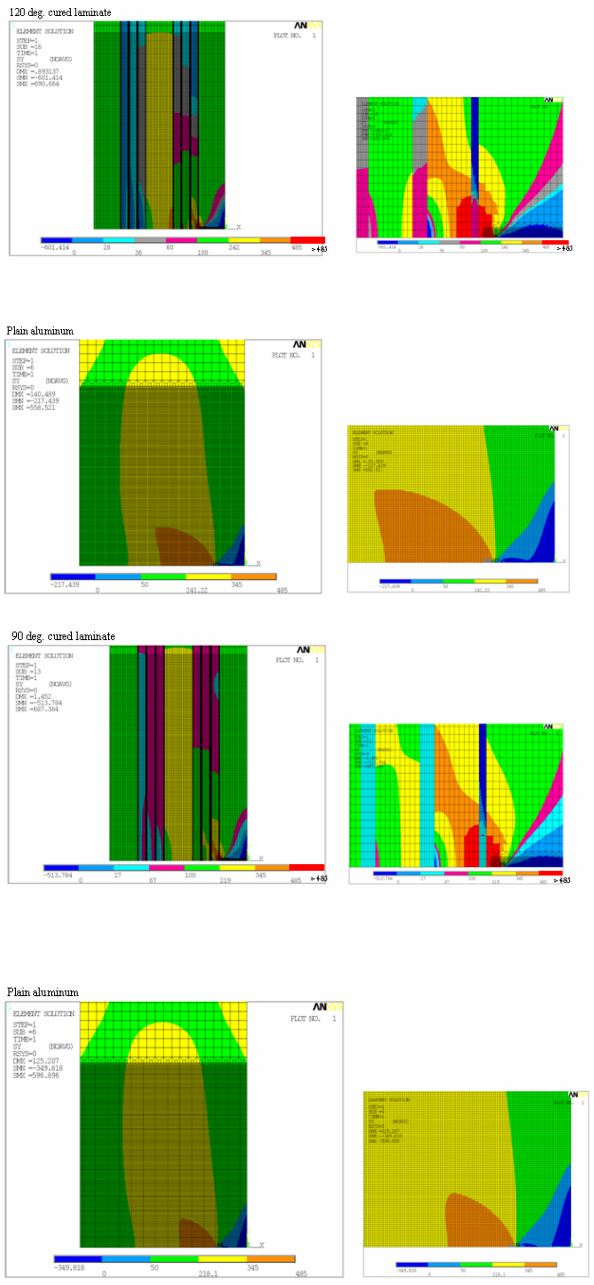

Figure-5. Sample stress plots in y direction, $\sigma_{y,total}$, near Mode I crack tip in Type I laminates and plain aluminum specimens.

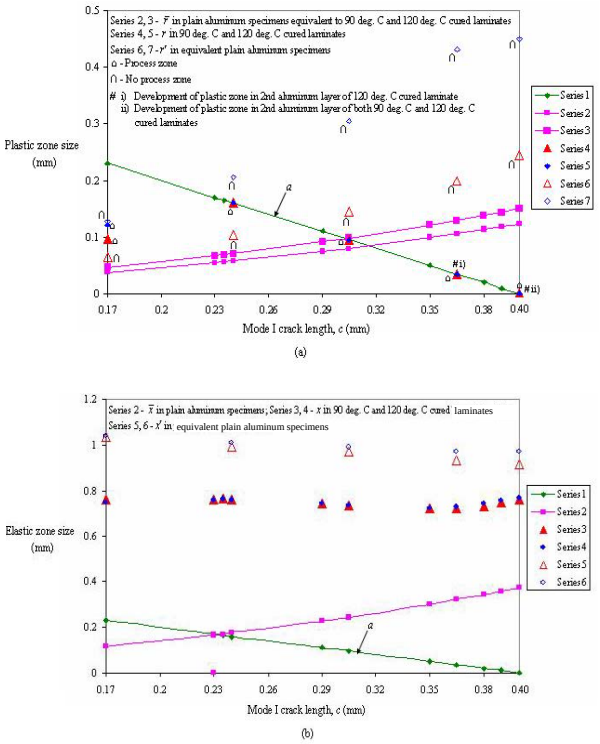

Figure-6. Plastic and elastic zone sizes *vs* Mode I crack length in Type I laminate and plain aluminum specimens.

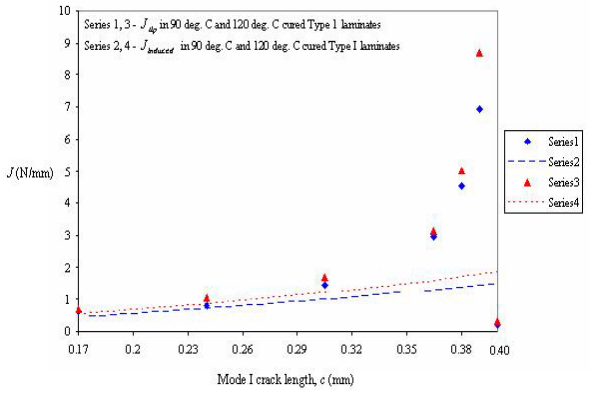

Figure-7. Energy release rates *vs* Mode I crack length in Type I laminate.

Type II laminate
Multiple delaminations
120 deg. C cured

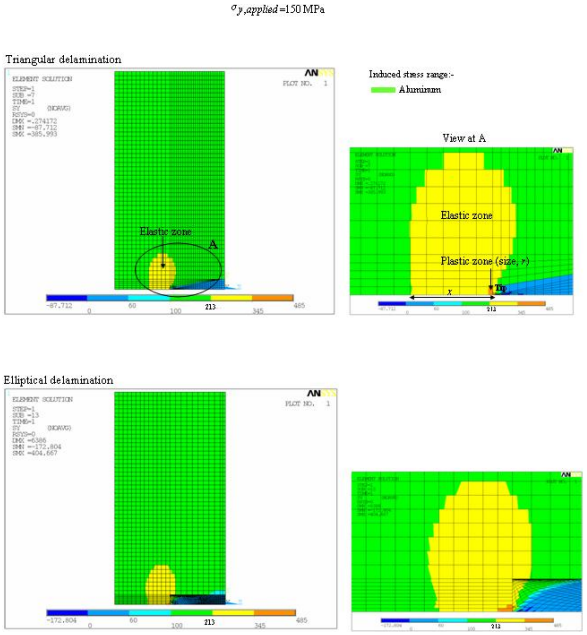

90 deg. C cured

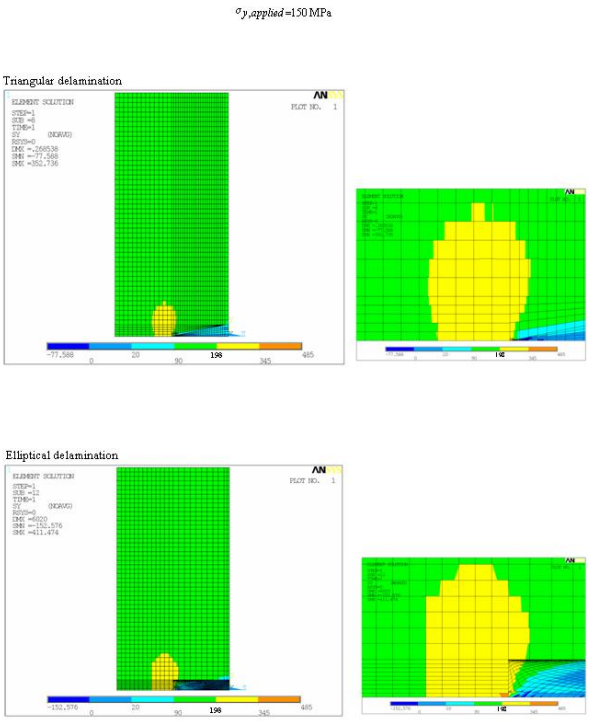

Double delamination
120 deg. C cured

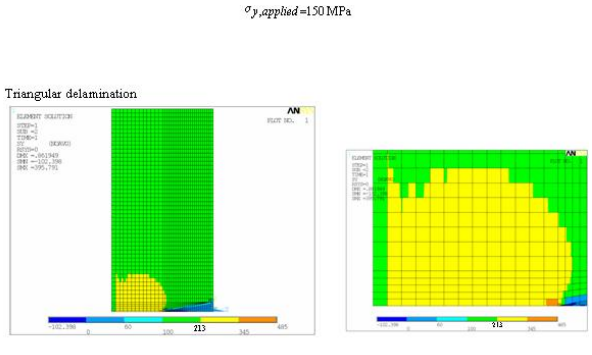

90 deg. C cured

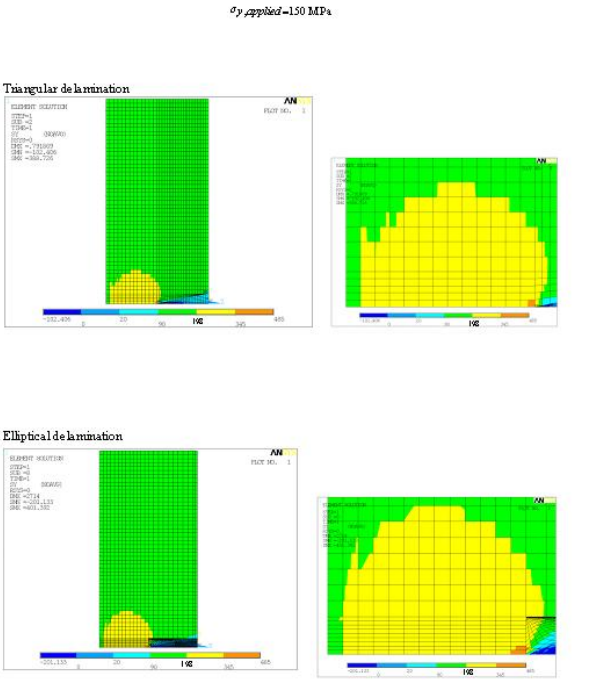

Plain aluminum specimen
(Equivalent. to 90 deg. C cured laminate)

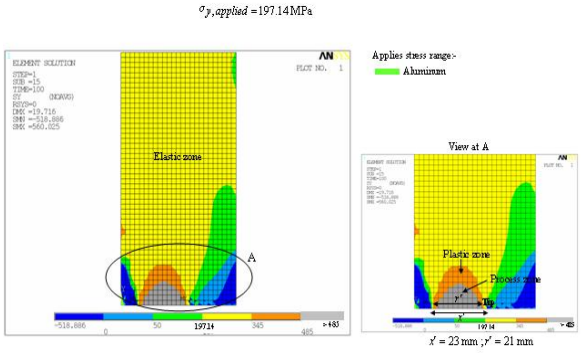

Figure-8. Stress plots in *y* direction, $\sigma_{y,total,al}$, near mode I crack tip in aluminum layer of Type II laminates and plain aluminum specimens.

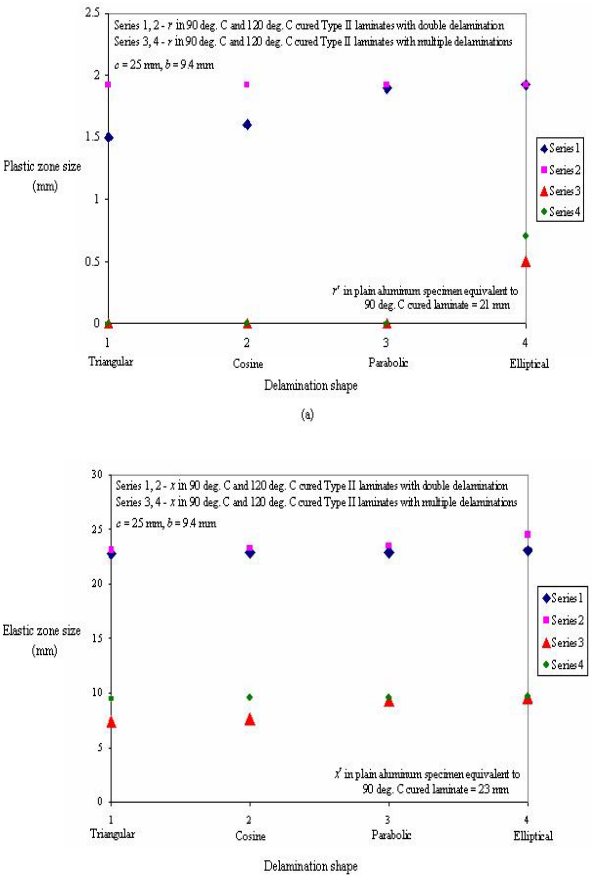

Figure-9. Plastic and elastic zone sizes *vs* delamination shape in Type II laminate and plain aluminum specimens.

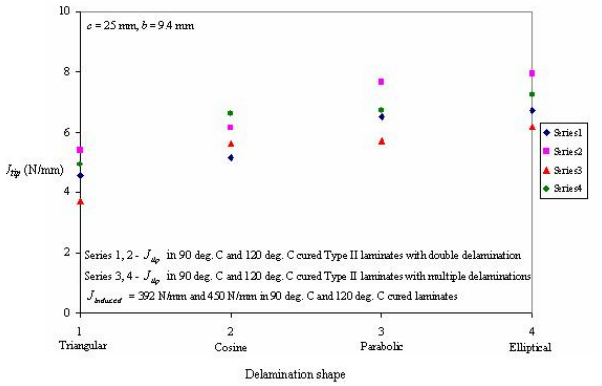

Figure-10. Crack tip energy release rate *vs* delamination shape in Type II laminate.

7. CONCLUSIONS

Glare laminates, comprising 2024-T3 aerospace aluminum alloy layers alternately bonded with epoxy resin impregnated E-glass fibre based composite prepregs, having different Mode I crack configurations - Type I and Type II are modeled by finite element method under the action of monotonic tensile stress, with SSY condition at the crack tips, to observe the effect of property mismatch between un-identical materials of the laminate over the nature and the size of the crack tip zones. Similarly stressed, plain 2024-T3 aerospace aluminum alloy specimens with same dimensions and crack configurations as that of the laminates are also modeled for the purpose of comparison. The following inferences are drawn from the results reported in the paper:

i) Load transfer towards Mode I crack on reaching near the interface of prepreg in Type I laminate changes the shape of crack tip zones vis-à-vis in plain aluminum specimens. Amplification of crack tip stress field in the laminate leads to the formation of process zone that is not found to develop in plain aluminum specimen. Values of J_{tip} are more than $J_{induced}$ in the laminate due to the amplification effect. The trend reverses to shielding when the crack tip touches the interface of soft resin of the prepreg.

ii) Load transfer away from Mode I cracks towards the fibres in Type II laminate (fibre bridging) results in shielding effect at the crack tips that diminishes the size of crack tip zones vis-à-vis in plain aluminum specimens. Reduction of crack tip stress field in the laminate eliminates the process zone that is found to exist in plain aluminum specimen. Values of J_{tip} are less than $J_{induced}$ in the laminate due to fibre bridging effect. Crack tip shielding is found to be more in multiple than in double delamination type laminates and is maximum in the case of triangular delamination and least in the case of elliptical delamination in both double and multiple delamination type laminates.

iii) Stated effects in both Type I and Type II laminates are more in the case of 120 deg. cured laminate (with higher residual stress) than in the case of 90 deg. cured laminate (with lower residual stress). In other words, the residual stress intensifies the effects.

ACKNOWLEDGEMENTS

The authors are thankful to Science and Engineering Research Council, Department of Science and Technology, India for funding the project. Help received from the School of Mechanical and Building Sciences, VIT University, India during the course of this work is appreciated.

REFERENCES

[1] Kim A. S., Suresh S. and Shih C. F. 1997. Plasticity effects on fracture normal to interfaces with homogeneous and graded compositions. Int. J. Sol. and Str. 34: 3415-3432.

[2] Kim A. S., Besson J. and Pineau A. 1999. Global and local approaches to fracture normal to interfaces. Int. J. Sol. and Str. 36: 1845-1864.

[3] Milan M. T. and Bowen P. 2003. Experimental and predicted fatigue crack growth resistance in Al 2124/Al 2124+35% SiC (3 μm) bi-material. Int. J. Fat. 25: 649-659.

[4] Predan J., Gubeljak N. and Kolednik O. 2007. On the local variation of the crack driving force in a double mismatched weld. Eng. Fra. Mech. 74: 1739-1757.

[5] Bhat S. and Patibandla R. 2013. Examination of small crack normal to multiple elasticity and plasticity mismatched interfaces in residually stressed fibre metal laminate (Glare): Theoretical and numerical approaches. Int. J. Dam. Mech. 22: 405-439.

[6] Guo Y. J. and Wu X. R. 1998. A theoretical model for predicting fatigue crack growth rates in fibre-reinforced metal laminates. Fat. Frac. Engg. Mat. Str. 21: 1133-1145.

[7] Guo Y. J. and Wu X. R. 1999. Phenomenological model for predicting crack growth in fibre reinforced metal laminates under constant amplitude loading. Com. Sci. and Tech. 59: 1825-1831.

[8] Guo Y. J. and Wu X. R. 1999. Bridging stress distribution in center-cracked fibre reinforced metal laminate: Modeling and Experiment. Eng. Fra. Mech. 63: 147-163.

[9] Alderliesten R. C. and Homan J. J. 2006. Fatigue and damage tolerance issues of Glare in aircraft structures. Int. J. Fat. 28: 1116-1123.

[10] Alderliesten R. C. 2007. Analytical prediction model for fatigue crack propagation and delamination growth in Glare. Int. J. Fat. 29: 628-646.

[11] Alderliesten R. C. 2007. On the available relevant approaches for fatigue crack propagation prediction in Glare. Int. J. Fat. 29: 289-304.

[12] Alderliesten R. C. and Rans C. 2009. The meaning of threshold fatigue in fibre metal laminates. Int. J. Fat. 31: 213-222.

[13] Rice J. R. 1968. A path independent integral and approximate analysis of strain concentration by notches and cracks. J. App. Mech. 35: 379-386.

[14] Tantina G. G. and DeLorenzl H. G. Elastic plastic fracture mechanics analysis of small cracks. Report, General Electric Corporate Research and Development, Schenectady, New York, USA. 12301: 207.

APPENDIX -A

Stress-strain data of un-cracked Glare

Type I (*y-z* plane)

Residual stress in material layer, *m*, is found as follows by using
$T_{ambient} = 30\,\text{deg.C}$ and $T_{curing} = 90\,\text{deg.C}$ and $120\,\text{deg.C}$:-

Residual strain, $\{\varepsilon\}_{m,rs} = \left[\begin{Bmatrix}\alpha_z\\ \alpha_y\\ 0\end{Bmatrix}_m - \begin{Bmatrix}\alpha_{ll}\\ \alpha_{ll}\\ 0\end{Bmatrix}\right] \times \left(T_{curing} - T_{ambient}\right)$;

Residual stress, $\{\sigma\}_{m,rs} = \{\mathrm{M}\}_m \times \{\varepsilon\}_{m,rs}$

Properties of aluminum, *al*, resin, *r*, and fibre, *f*, are used in place of *m*. Since *z* dimension is very small, residual stress in *z* direction is assumed to be zero in all the material layers. Stiffness matrices are as follows:

$$\{\mathrm{M}\}_{al} = \begin{bmatrix}105.0 & 52.53 & 0\\ 52.53 & 105.0 & 0\\ 0 & 0 & 27.06\end{bmatrix}\text{GPa}$$

$$\{\mathrm{M}\}_{r} = \begin{bmatrix}5.108 & 2.554 & 0\\ 2.554 & 5.108 & 0\\ 0 & 0 & 1.25\end{bmatrix}\text{GPa}$$

$$\{\mathrm{M}\}_{f} = \begin{bmatrix}81.05 & 22.86 & 0\\ 22.86 & 81.05 & 0\\ 0 & 0 & 29.71\end{bmatrix}\text{GPa}$$

$$\{\mathrm{M}\}_{lam} = \{\mathrm{M}\}_{al} \times \frac{t_{al} \times 3}{d} + \{\mathrm{M}\}_{f} \times \frac{t_f \times 6}{d} + \{\mathrm{M}\}_{r} \times \frac{t_r \times 12}{d}$$

where t_{al}, t_f and t_r are the thickness of aluminum, fibre and resin layers. t_{al} = 0.4 mm, t_f = 0.1 mm and t_r = 0.0165 mm. Constants 3, 6 and 12 represent the number of respective layers.

$$\{\mathrm{M}\}_{lam} = \begin{bmatrix}87.82 & 38.62 & 0\\ 38.62 & 87.82 & 0\\ 0 & 0 & 25.27\end{bmatrix}\text{GPa}$$

$$\{\mathrm{M}\}_{lam}^{-1} = \begin{bmatrix}0.01411 & -0.0062 & 0\\ -0.0062 & 0.01411 & 0\\ 0 & 0 & 0.0395\end{bmatrix}$$

For $\sigma_{applied}$ $= \begin{Bmatrix}\sigma_z\\ \sigma_y\\ \tau_{zy}\end{Bmatrix}_{applied} = \begin{Bmatrix}0\\ 150\\ 0\end{Bmatrix}$ MPa

$$\varepsilon_{lam} = \begin{Bmatrix}\varepsilon_z\\ \varepsilon_y\\ \gamma_{zy}\end{Bmatrix}_{lam} = \{\mathrm{M}\}_{lam}^{-1}\sigma_{applied} = \begin{Bmatrix}-9.3\times10^{-4}\\ 2.11\times10^{-3}\\ 0\end{Bmatrix}$$

Induced stresses in material layer, *m*,

$$\{\sigma\}_{induced,m} = \begin{bmatrix}\sigma_z\\ \sigma_y\\ \tau_{yz}\end{bmatrix}_{induced,m} = \{\mathrm{M}\}_m \times \left[\{\varepsilon\}_{m,rs} + \varepsilon_{lam}\right]$$

and $\sigma_{x,m} = \upsilon_m(\sigma_z + \sigma_y)_{induced,m}$

w/o rs 90deg.C 120deg.C

$$\{\sigma\}_{induced,al} = \left[\begin{Bmatrix}0.0\\ 173.37\\ 0\end{Bmatrix}\begin{Bmatrix}0.0\\ 218.1\\ 0\end{Bmatrix}\begin{Bmatrix}0.0\\ 241.22\\ 0\end{Bmatrix}\right]\text{MPa}$$

σ_x = 57.21 71.97 79.6

Residual stresses at 90 deg. C curing = 14.76 MPa (+ve) in *x* dir., 44.73 MPa (+ve) in *y* dir.
Residual stresses at 120 deg. C curing = 22.39 MPa (+ve) in *x* dir., 67.85 MPa (+ve) in *y* dir.

w/o rs 90deg. C 120deg. C

$$\{\sigma\}_{induced,r} = \left[\begin{Bmatrix}0.0\\ 8.43\\ 0\end{Bmatrix}\begin{Bmatrix}0.0\\ 26.47\\ 0\end{Bmatrix}\begin{Bmatrix}0.00\\ 35.48\\ 0\end{Bmatrix}\right]\text{MPa}$$

σ_x = 2.78 8.73 11.7

Residual stresses at 90 deg. C curing = 5.95 MPa (+ve) in *x* dir., 18.04 MPa (+ve) in *y* dir.
Residual stresses at 120 deg. C curing = 8.92 MPa (+ve) in *x* dir., 27.05 MPa (+ve) in *y* dir.

w/o rs 90deg.C 120deg.C

$$\{\sigma\}_{induced,f} = \left[\begin{Bmatrix}0.0\\150.28\\0\end{Bmatrix}\begin{Bmatrix}0.0\\66.49\\0\end{Bmatrix}\begin{Bmatrix}0.0\\26.25\\0\end{Bmatrix}\right] \text{MPa}$$

$\sigma_x =$ 33.06 14.62 5.77

Residual stresses at 90 deg. C curing = 18.44 MPa (-ve) in *x* dir., 83.79 MPa (-ve) in *y* dir.
Residual stresses at 120 deg. C curing = 27.29 MPa (-ve) in *x* dir., 124.03 MPa (-ve) in *y* dir.

Again due to small laminate thickness, stiffness in *z* direction is negligible and induced stress in *z* direction is considered to be zero in all the material layers.

Type II (*x*-*y* plane)

Residual strain, $\{\varepsilon\}_{m,rs} = \left[\begin{Bmatrix}\alpha_x\\\alpha_y\\0\end{Bmatrix}_m - \begin{Bmatrix}\alpha_{tl}\\\alpha_{ll}\\0\end{Bmatrix}\right] \times \left(T_{curing} - T_{ambient}\right)$

Residual stress, $\{\sigma\}_{m,rs} = \{\mathrm{M}\}_m \times \{\varepsilon\}_{m,rs}$

$$\{\mathrm{M}\}_{al} = \begin{bmatrix}80.79 & 26.66 & 0\\26.66 & 80.79 & 0\\0 & 0 & 27.06\end{bmatrix} \text{GPa}$$

$$\{\mathrm{M}\}_{r} = \begin{bmatrix}3.92 & 1.29 & 0\\1.29 & 3.92 & 0\\0 & 0 & 1.25\end{bmatrix} \text{GPa}$$

$$\{\mathrm{M}\}_{f} = \begin{bmatrix}74.61 & 16.41 & 0\\16.41 & 74.61 & 0\\0 & 0 & 29.70\end{bmatrix} \text{GPa}$$

$$\{\mathrm{M}\}_{lam} = \begin{bmatrix}71.22 & 21.04 & 0\\21.04 & 71.22 & 0\\0 & 0 & 25.26\end{bmatrix} \text{GPa}$$

$$\{\mathrm{M}\}_{lam}^{-1} = \begin{bmatrix}0.0153 & -0.0045 & 0\\-0.0045 & 0.0153 & 0\\0 & 0 & 0.0395\end{bmatrix}$$

For $\sigma_{applied}$ = $\begin{Bmatrix}\sigma_x\\\sigma_y\\\tau_{xy}\end{Bmatrix}_{applied} \begin{Bmatrix}0\\150\\0\end{Bmatrix}$ MPa

$$\varepsilon_{lam} = \begin{Bmatrix}\varepsilon_x\\\varepsilon_y\\\gamma_{xy}\end{Bmatrix}_{lam} = \begin{Bmatrix}-6.75\times10^{-4}\\2.29\times10^{-3}\\0\end{Bmatrix}$$

Induced stresses in material layer (*m*),

$$\{\sigma\}_{induced,m} = \begin{bmatrix}\sigma_x\\\sigma_y\\\tau_{xy}\end{bmatrix}_{induced,m} = \{\mathrm{M}\}_m \times \left[\{\varepsilon\}_{m,rs} + \varepsilon_{lam}\right]$$

w/o rs 90deg.C 120deg.C

$$\{\sigma\}_{induced,al} = \left[\begin{Bmatrix}6.50\\167.0\\0\end{Bmatrix}\begin{Bmatrix}41.32\\197.14\\0\end{Bmatrix}\begin{Bmatrix}58.79\\212.6\\0\end{Bmatrix}\right] \text{MPa};\ \sigma_z = 0$$

Residual stresses at 90 deg. C curing = 34.82 MPa (+ve) in *x* dir., 30.14 MPa (+ve) in *y* dir.
Residual stresses at 120 deg. C curing = 52.29 MPa (+ve) in *x* dir., 45.6 MPa (+ve) in *y* dir.

w/o rs 90deg.C 120deg.C

$$\{\sigma\}_{induced,r} = \left[\begin{Bmatrix}0.308\\8.1\\0\end{Bmatrix}\begin{Bmatrix}12.78\\20.35\\0\end{Bmatrix}\begin{Bmatrix}19.00\\26.45\\0\end{Bmatrix}\right] \text{MPa};\ \sigma_z = 0$$

Residual stresses at 90 deg. C curing = 12.47 MPa (+ve) in *x* dir., 12.25 MPa (+ve) in *y* dir.
Residual stresses at 120 deg. C curing = 18.69 MPa (+ve) in *x* dir., 18.35 MPa (+ve) in *y* dir.

w/o rs 90deg.C 120deg.C

$$\{\sigma\}_{induced,f} = \left[\begin{Bmatrix}-12.78\\159.78\\0\end{Bmatrix}\begin{Bmatrix}-81.0\\86.53\\0\end{Bmatrix}\begin{Bmatrix}-114.87\\50.7\\0\end{Bmatrix}\right] \text{MPa};\ \sigma_z = 0$$

Residual stresses at 90 deg. C curing = 68.22 MPa (-ve) in *x* dir., 73.25 MPa (-ve) in *y* dir.
Residual stresses at 120 deg. C curing = 102.09 MPa (-ve) in *x* dir., 109.08 MPa (-ve) in *y* dir.

w/o : Without residual stress
+ve : Tensile stress
-ve : Compressive stress